Electronic Supplementary Information for Dalton Transactions

Cobalt(II)-octacyanotungstate(V) organic-inorganic hybrid ferromagnetic materials with pyrazine and 4,4'-bipyridine

Robert Podgajny,[a*] Maria Bałanda,[b] Marcin Sikora,[c] Marta Borowiec,[c] Leszek Spałek,[d] Czesław Kapusta,[c] and Barbara Sieklucka[a *]

[a] *Faculty of Chemistry, Jagiellonian University, Ingardena 3, 30-060 Kraków, Poland, e-mail: podgajny@chemia.uj.edu.pl, siekluck@chemia.uj.edu.pl*

[b] *H. Niewodniczański Institute of Nuclear Physics PAN, Radzikowskiego 152, 31-342 Kraków, Poland*

[c] *Faculty of Physics and Applied Computer Science, AGH – University of Science and Technology, Mickiewicza 30, 30-059 Kraków, Poland*

[d] *Cavendish Laboratory, University of Cambridge, Cambridge CB3 0HE, United Kingdom*

Supplementary Information

Table of contents

bpy)$[W(CN)_8]_4\}^{4-}$ (**2b**) and $\{Co_4(DMF)_3(H_2O)_7$(4,4'-bpy)$_2[W(CN)_8]_4\}^{4-}$ (**2c**) aggregates.

Table S6. Isotopic pattern of multi-lines bands assigned to the $\{Co_2(H_2O)_6$(4,4'-bpy)$[W(CN)_8]_2\}^{2-}$ (**2d**) and $\{Co_2(DMF)_4[W(CN)_8]_2\}^{2-}$ (**2e**) products of fragmentation within the band of m/z = 607.88.

Table S7. The interpretation of fragmentation spectrum of m/z = 607.88.

Figure S1. The **c**omparison of IR spectra of **pyz** (condensed phase) and **1** range 1200 – 900 cm^{-1}.

Figure S2. The comparison of IR spectra of **4,4'-bpy** (condensed phase) and **2** range 700 – 500 cm^{-1}.

Figure S3. The comparison of IR spectra of **4,4'-bpy** (condensed phase) and **2** range 1100 - 800 cm^{-1}.

Figure S4. Reflectance electronic spectra of solids **1** (red), **2** (green) and mixture of solids $CoSO_4{\cdot}7H_2O$ and 4,4'-bpy (blue) recorded at ambient temperature.

Figure S5. TGA coupled with QMS analyses for **1** (left) and **2** (right).

Figure S6. The fragmentation spectra of m/z = 607.88 band.

Figure S7. The representative fragment of ES-MS spectrum showing multi-lines bands assigned to set of doubly charged $[W(CN)_x]^{2-}$ species.

Figure S8. Thermal dependence of molar magnetisation for **1** and **2** measured at H_{dc} = 2 kOe. Inset: magnetisation change of **1** during the cooling of the sample in the field of superconducting magnet (ca. 10 Oe).

Table S1. IR spectra of **1**, **2** and related *spacer* ligands

pyz[a]	pyz[b]	**1**	4,4'-bpy[c]	4,4'-bpy[d]	**2**	Assignment[e]
		3394vs(v.br.)			3444s(v.br.)	ν(O–H)
3066w	3064s	2962vw		2965s	2964vw	ν(ArC-H)
2973w	2970w	2925w		2926vs	2927w	
		2851vw		2850s	2852vw	
		2180m(sh)			2197(sh)	ν(C≡N)
		2156s			2184(sh)	
		2144m(sh)			2173m	
					2154m	
					2123m	
		1651s			1653m	γ(O-H),
		1624m(sh)		1604w	1608vs	
			1593s	1594s		(ArC=C)
					1535m	
			1535s	1535m		
1490s	1491w	1491vw			1491m	
			1490s	1491m		
1418vs	1415vs	1418vs				
				1465s		
		1381w			1413s	
			1416m	1412s		
1342m	1342w				1380w	
				1380m		
	1240vw	1256vw			1322w	
		1236vw				
1178m	1178w	1158m	1221s	1221m	1223m	γ(ArCH in-plane)
1148vs	1150s		1176w			ring breathing,
1125w	1125w	1126m		1133vw		ring deformation,
1110m	1105w		1102m	1102vw	1106w	γ(ArCH out-of-plane)
			1079s	1079m	1068m	
1067vs	1068s	1083w	1043m	1044w	1045w	
1048vw		1051s	995s	992m	1005w	
1032vw			982m	983w		
1022m	1021vs	1026w	968m	968w		
1006m						
926vw						
823vw			882m	884w		
804vs	805w(sh)	803m	853w	855w	856w	
789w	795vs		800vs	807m	810s	
752vw				747w		
700vw			736s	736w	730w	
597w				724w		
					634m	Ring deformation,
			618s	612s	621(sh)	
				570w	574w	Coordination,
		484w(sh)	508s	502w	473m(v.br.)	
		471m				
417m	416m	450m				

[a] The IR pattern of pyz was adapted from ref. 54.[b] The IR spectra of pyz in solid state. [c]The IR pattern of free 4,4'-bpy was adapted form ref. 55. [d] The IR spectra of pyz in solid state. [e]The bands of pyz and 4,4'-bpy and were assigned according to the refs. 54,55.

Table S2. Isotopic pattern of multi-lines bands assigned to the $\{Co_2(DMF)_2[W(CN)_8]_2\}^{2-}$ (**1a**), $\{Co_2(H_2O)W(CN)_8\}^{-}$ (**1b**) and $\{Co_2(pyz)_2[W(CN)_8]_2\}^{2-}$ (**1c**) aggregates.

1a		**1b**		**1c**	
$(m/z)_{exp}$	$(m/z)_{calc}$ (Int. / %)	$(m/z)_{exp}$	$(m/z)_{calc}$ (Int. / %)	$(m/z)_{exp}$	$(m/z)_{calc}$ (Int. / %)
	520.96 (0.23)		523.85(0.37)		527.94 (0.22)
	521.46 (0.19)		524.85 (0.04)		528.44 (0.20)
521.92	521.96 (25.29)	525.95	525.85 (81.46)	528.95	528.94 (25.01)
522.48	522.46 (34.74)	526.95	526.85 (53.50)	529.28	529.44 (35.03)
523.00	522.96 (74.84)	527.95[a]	527.85 (100.00) (max)	530.00	529.94 (74.83)
523.52	523.46 (52.74)	528.95	528.85 (11.40)	530.45	530.44 (54.03)
523.95 (max)	523.96 (100.00) max	530.00	529.85 (88.20)	530.98[a]	530.94 (100.00) max
524.50	524.46 (57.61)	530.98	530.85 (10.25)	531.45	531.44 (59.45)
524.95	524.96 (75.41)		531.85 (0.73)	531.92	531.94 (75.73)
525.48	525.46 (20.99)		532.85 (0.04)	532.52	532.44 (22.56)
525.95	525.96 (32.05)			532.98	532.94 (31.96)
526.45	526.46 (9.20)			533.48	533.44 (9.88)
526.95	526.96 (1.47)			533.95	533.94 (1.57)
	527.46 (0.17)				534.44 (0.17)

[a]The expected maxima are not of the highest intensity due to the overlap of bands of close *m*/*z* values.

Table S3. Isotopic pattern of multi-lines bands assigned to the $\{Co_4(CN)_4(H_2O)_5(pyz)_2[W(CN)_8]_2\}^{2-}$ (**1d**) $\{Co_4(CN)_4(DMF)_2(H_2O)_2(pyz)_4[W(CN)_8]_2\}^{2-}$ (**1e**) $\{Co_4(CN)_4(DMF)_3(pyz)_4[W(CN)_8]_2\}^{2-}$ (**1f**) and $\{Co_4(CN)_4(DMF)_3(H_2O)_2(pyz)_4[W(CN)_8]_2\}^{2-}$ (**1g**) aggregates.

1d		**1e**		**1f**		**1g**	
$(m/z)_{exp}$	$(m/z)_{calc}$	$(m/z)_{exp}$	$(m/z)_{calc}$	$(m/z)_{exp}$	$(m/z)_{calc}$	$(m/z)_{exp}$	$(m/z)_{calc}$
	683.91		809.98		828.5		846.51
684.3	684.41	810.3	810.48		829.0	846.8	847.01
884.8	684.91	810.9	810.98	829.6	829.5	847.5	847.51
685.5	685.41	811.6	811.48	830.0	830.0	848.1	848.01
686.0	685.91	812.1	811.98	830.7	830.5	848.6	848.51
686.6	686.41	812.7	812.48	831.1	831.0	849.3	849.01
687.1 (max)	686.91 (max)	813.1	812.98 (max)	831.7	831.5 (max)	849.7 (max)	849.51 (max)
687.6	687.41	813.6 (max)	813.48	832.1 (max)	832.0	850.1	850.01
688.0	687.91	814.1	813.98	832.4	832.5	850.4	850.51
688.4	688.41	814.5	814.48	832.8	833.0	850.9	851.01
689.0	688.91	815.1	814.98	833.4	833.5	851.2	851.51
689.5	689.41	815.5	815.48	834.0	834.0	851.7	852.01
689.9	689.91	816.0	815.98	834.4	834.5	852.2	852.51
	690.41		816.48	835.1	835.0	852.9	853.01
	690.91		816.98		835.5		853.51

Table S4. Isotopic pattern of multi-lines bands assigned to the $\{Co(H_2O)_4[W(CN)_7]\}^-$ (**1h**), $\{Co[W(CN)_8]\}^-$ (**1i**) and $\{Co(H_2O)[W(CN)_8]\}^-$ (**1j**) aggregates.

1h		**1i**		**1j**	
$(m/z)_{exp}$	$(m/z)_{calc}$ (Int. / %)	$(m/z)_{exp}$	$(m/z)_{calc}$ (Int. / %)	$(m/z)_{exp}$	$(m/z)_{calc}$ (Int. / %)
	492.94 (0.37)		446.9 (0.37)		444.9 (0.37)
	493.94 (0.04)		447.9 (0.04)		445.9 (0.04)
495.2	494.94 (81.59)	449.35	448.9 (81.63)	449.35	446.9 (81.63)
496.2	495.94 (52.56)	450.42	449.9 (53.55)	450.42	447.9 (53.55)
497.1 (max)	496.94 (100.00) (max)	451.38 (max)	450.9 (100.00) (max)	451.38 (max)	468.9 (100.00) (max)
497.95	497.94 (10.50)	452.6	451.9 (11.25)	452.6	469.9 (11.25)
498.98	498.94 (88.82)	453.2	452.9 (88.17)	453.2	470.9 (88.17)
499.92	499.94 (9.23)		453.9 (10.18)		471.9 (10.18)
	500.94 (1.16)		454.9 (0.54)		472.9 (0.54)
	501.94 (0.01)		455.9 (0.02)		473.9 (0.02)

Table S5. Isotopic pattern of multi-lines bands assigned to the $\{Co_2(DMF)_2(H_2O)_6[W(CN)_8]_2\}^{4-}$ (**2a**), $\{Co_4(DMF)_4(H_2O)_{10}(4,4'\text{-bpy})[W(CN)_8]_4\}^{4-}$ (**2b**) and $\{Co_4(DMF)_3(H_2O)_7(4,4'\text{-bpy})_2[W(CN)_8]_4\}^{4-}$ (**2c**) aggregates.

2a		**2b**		**2c**	
$(m/z)_{exp}$	$(m/z)_{calc}$ (Int. / %)	$(m/z)_{exp}$	$(m/z)_{calc}$ (Int. / %)	$(m/z)_{exp}$	$(m/z)_{calc}$ (Int. / %)
	287.49(0.22)	605.50	605.50 (0.03)	612.81	612.75 (0.03)
287.81	287.74 (0.19)	605.75	605.75 (0.08)	613.00	613.00 (0.08)
288.00	287.99 (25.01)		606.00 (2.01)	613.25	613.25 (1.95)
288.25	288.24 (34.45)	606.25	606.25 (5.52)	613.44	613.50 (5.41)
288.43	288.49 (74.45)	606.50	606.50 (15.43)	613.68	613.75 (15.13)
288.81	288.74 (52.86)	606.81	606.75 (25.06)	613.94	614.00 (24.84)
289.06 (max)	288.99 (100.00) max	607.12	607.00 (45.13)	614.31	614.25 (44.62)
289.31	289.24 (57.99)		607.25 (57.64)	614.56	614.50 (57.52)
289.62	289.49 (76.02)	607.50	607.50 (82.10)	614.81 (max)	614.75 (81.64)
289.87	289.74 (21.75)	607.75	607.75 (84.94)	615.00	615.00 (85.36)
290.12	289.99 (32.70)	607.88(max)	608.00 (100.00)(max)	615.31	615.25 (100.00) (max)
290.38	290.24 (9.48)	608.25	608.25 (86.88)	615.56	615.50 (87.93)
	290.49 (1.88)	608.50	608.50 (87.82)	615.75	615.75 (88.28)
	290.74 (0.28)		608.75 (63.37)	615.94	616.00 (64.71)
		608.88	609.00 (54.46)	616.31	616.25 (55.10)
		609.19	609.25 (33.16)	616.56	616.50 (34.18)
		609.38	609.50 (23.97)	616.87	616.75 (24.45)
		609.75	609.75 (11.80)	617.06	617.00 (12.33)
		610.06	610.00 (6.50)	617.25	617.25 (6.73)
		610.31	610.25 (2.87)	617.56	617.50 (3.02)
		610.62	610.50 (0.95)		617.75 (1.03)
		610.81	610.75(0.25)	617.94	618.00(0.28)
		611.12	611.00(0.05)		618.25(0.06)

Table S6. Isotopic pattern of multi-lines bands assigned to the $\{Co_2(H_2O)_6(4,4'\text{-bpy})[W(CN)_8]_2\}^{2-}$ (**2d**) and $\{Co_2(DMF)_4[W(CN)_8]_2\}^{2-}$ (**2e**) products of fragmentation within the band of *m*/*z* = 607.88.

2d		**2e**	
$(m/z)_{exp}$	$(m/z)_{calc}$ (Int. / %)	$(m/z)_{exp}$	$(m/z)_{calc}$ (Int. / %)
	579.97(0.22)	593.9	594.01(0.22)
580.6	580.47 (0.20)	594.3	594.51 (0.20)
580.9	580.97 (24.54)	594.9	595.01 (24.23)
581.4	581.47 (34,8)	595.3	595.51 (35,07)
582.0	581.97 (74,35)	595.8	596.01 (74,30)
582.4	582.47 (54,78)	596.3	596.51 (56,09)
582.9 (max)	582.97 (100,00) max	597.00 (max)	597.01 (100,00) (max)
583.3	583.47 (60,80)	597.4	597.51 (62,69)
583.9	583.97 (76,60)	598.1	598.01 (76,98)
584.5	584.47 (24,24)		598.51 (25,91)
584.9	584.97 (32,70)	598.8	599.01 (32,69)
585.5	585.47 (10,56)	599.3	599.51 (11,27)
586.1	585.97 (2,12)	599.9	600.01 (2,28)
	586.47 (0,32)	600.4	600.51 (0,33)

Table S7. The interpretation of fragmentation spectrum of m/z = 607.88.

$\{Co_2(H_2O)_6(4,4'\text{-bpy})[W(CN)_8]_2\}^{2-}$ (2d)	**$(m/z)_{exp}$ = 582.9** **$(m/z)_{calc}$ = 582.97** **m_{calc} = 1165.94 a.u.**	**$\{Co_2(DMF)_4[W(CN)_8]_2\}^{2-}$ (2e)**	**$(m/z)_{exp}$ = 597.0** **$(m/z)_{calc}$ = 597.01** **m_{calc} = 1194.02 a.u.**
$\{Co_2(H_2O)_5(4,4'\text{-bpy})[W(CN)_8]_2\}^{2-}$	$(m/z)_{exp}$ = 572.9 $(m/z)_{calc}$ = 574 m_{calc} = 1148 a.u.	$\{Co_2(DMF)_2(H_2O)_5[W(CN)_8]_2\}^{2-}$	$(m/z)_{exp}$ = 568.5 $(m/z)_{calc}$ = 569 m_{calc} = 1138 a.u.
$\{Co_2(H_2O)_3(4,4'\text{-bpy})[W(CN)_8]_2\}^{2-}$	$(m/z)_{exp}$ = 555.8 $(m/z)_{calc}$ = 556.1 m_{calc} = 1112.2 a.u.	$\{Co_2(DMF)_3[W(CN)_8]_2\}^{2-}$	$(m/z)_{exp}$ = 561.5 $(m/z)_{calc}$ = 560.5 m_{calc} = 1121 a.u.
$\{Co_2[W(CN)_8]_2(H_2O)_2(4,4'\text{-bpy})\}^{2-}$	$(m/z)_{exp}$ = 547.9 $(m/z)_{calc}$ = 547 m_{calc} = 1094.0 a.u.	$\{Co_2[W(CN)_8]_2\}^{2-}$	$(m/z)_{exp}$ = 451.2 $(m/z)_{calc}$ = 450.9 m_{calc} = 901.8 a.u.
$\{Co_2(H_2O)(4,4'\text{-bpy})[W(CN)_8]_2\}^{2-}$	$(m/z)_{exp}$ = 538.6 $(m/z)_{calc}$ = 538 m_{calc} = 1076.0 a.u.	$\{Co_2[W(CN)_8][W(CN)_7]\}^{2-}$	$(m/z)_{exp}$ = 438.5 $(m/z)_{calc}$ = 437.9 m_{calc} = 875.8 a.u.
$\{Co_2(4,4'\text{-bpy})[W(CN)_8]_2\}^{2-}$	$(m/z)_{exp}$ = 529.5 $(m/z)_{calc}$ = 529 m_{calc} = 1058.0 a.u.	$\{Co_2[W(CN)_7]_2\}^{2-}$	$(m/z)_{exp}$ = 425.5 $(m/z)_{calc}$ = 424.9 m_{calc} = 849.88 a.u.
$\{Co_4(H_2O)_7(4,4'\text{-bpy})[W(CN)_8]_4\}^{4-}$	**$(m/z)_{exp}$ = 521.4** **$(m/z)_{calc}$ = 521.5** **m_{calc} = 2085.94 a.u.**	$\{Co_2[W(CN)_7][W(CN)_6]\}^{2-}$	$(m/z)_{exp}$ = 412.5 $(m/z)_{calc}$ = 411.9 m_{calc} = 823.8 a.u.
$\{Co_4(H_2O)_5(4,4'\text{-bpy})[W(CN)_8]_4\}^{4-}$	$(m/z)_{exp}$ = 513.1 $(m/z)_{calc}$ = 512.4 m_{calc} = 2049.6 a.u.	$\{Co_2[W(CN)_6]_2\}^{2-}$	$(m/z)_{exp}$ = 399.5 $(m/z)_{calc}$ = 398.9 m_{calc} = 797.8 a.u.
$\{Co_4(H_2O)_4(4,4'\text{-bpy})[W(CN)_8]_4\}^{4-}$	$(m/z)_{exp}$ = 509.7 $(m/z)_{calc}$ = 507.9 m_{calc} = 2031.6 a.u.		
$\{Co_4(H_2O)_3(4,4'\text{-bpy})[W(CN)_8]_4\}^{4-}$	$(m/z)_{exp}$ = 503.6 $(m/z)_{calc}$ = 503.4 m_{calc} = 2013.6 a.u.		
$\{Co_4(H_2O)(4,4'\text{-bpy})[W(CN)_8]_4\}^{4-}$	$(m/z)_{exp}$ = 495.1 $(m/z)_{calc}$ = 494.4 m_{calc} = 1980.4 a.u.		
$\{Co_4(4,4'\text{-bpy})[W(CN)_8]_4\}^{4-}$	$(m/z)_{exp}$ = 490.7 $(m/z)_{calc}$ = 489.7 m_{calc} = 1959.8 a.u.		

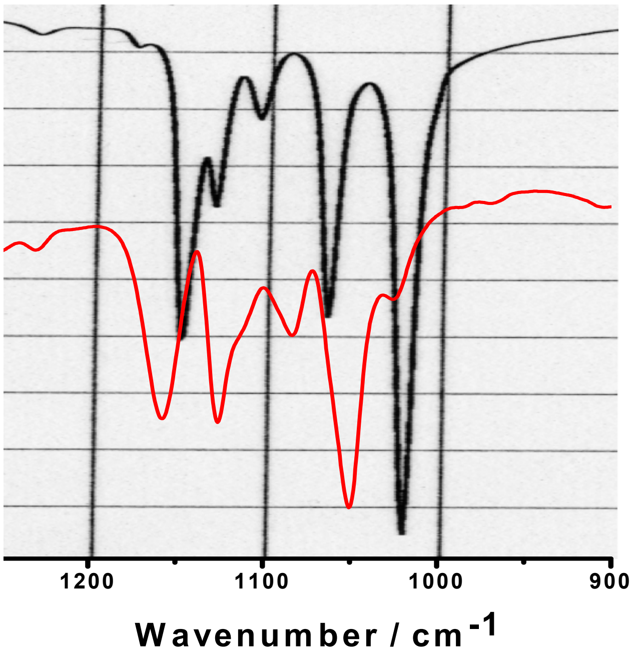

Black line: The IR spectrum of **pyz** condensed phase,	**Red line:** The IR spectrum of **1**
1178w	
1150vs	1158m
1125m	1126m
1105w	
	1083w
1068s	
	1051s
1021vs	1026w

Fig. S1. Comparison of IR spectra of **pyz** (condensed phase) and **1** range 1200 – 900 cm^{-1}

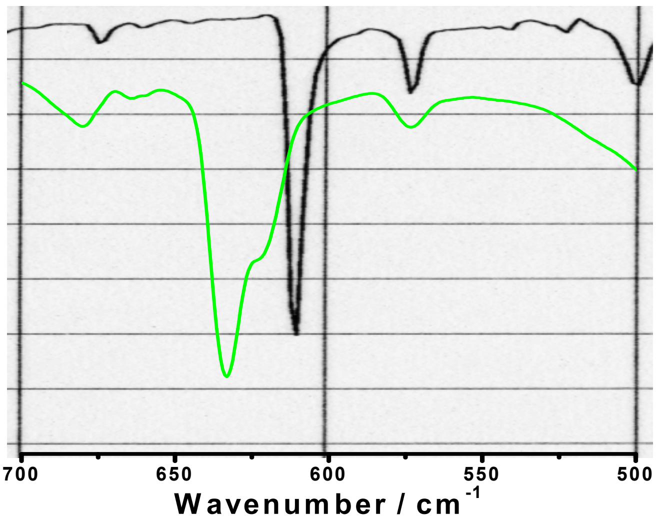

Black line: The IR spectrum of **4,4'-bpy** condensed phase,	**Green line:** The IR spectrum of **2**
612s	634m 621(sh)
573w	574w

Fig. S2. The comparison of IR spectra of **4,4'-bpy** (condensed phase) and **2** range 700 – 500 cm^{-1}

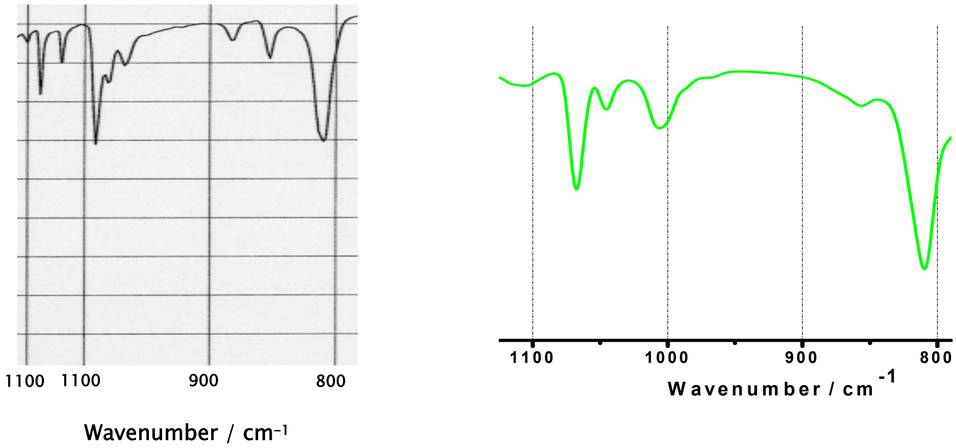

Black line: The IR spectrum of **4,4'-bpy** condensed phase,	**Green line:** The IR spectrum of **2**
1079w	1068m
1044w	1045w
992m	1005w
968w	
983w	
884w	
855w	856w
807m	810s

Fig. S3. The comparison of IR spectra of **4,4'-bpy** (condensed phase) and **2** range 1100 - 800 cm^{-1}

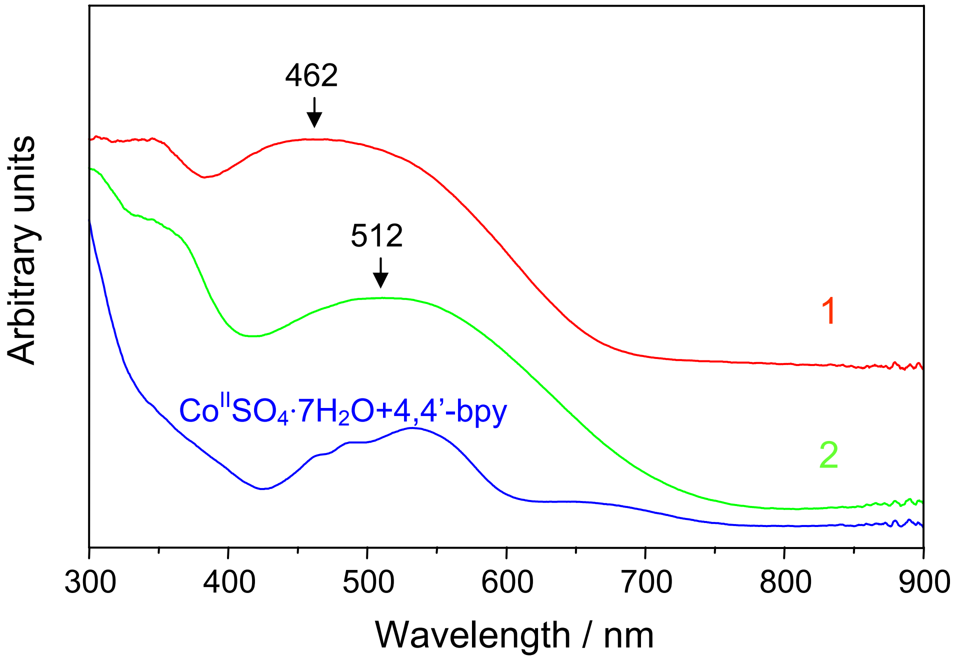

Fig. S4. Reflectance spectra of solids **1** (red), **2** (green) and mixture of solids $CoSO_4·7H_2O$ and 4,4'-bpy (blue) recorded at ambient temperature.

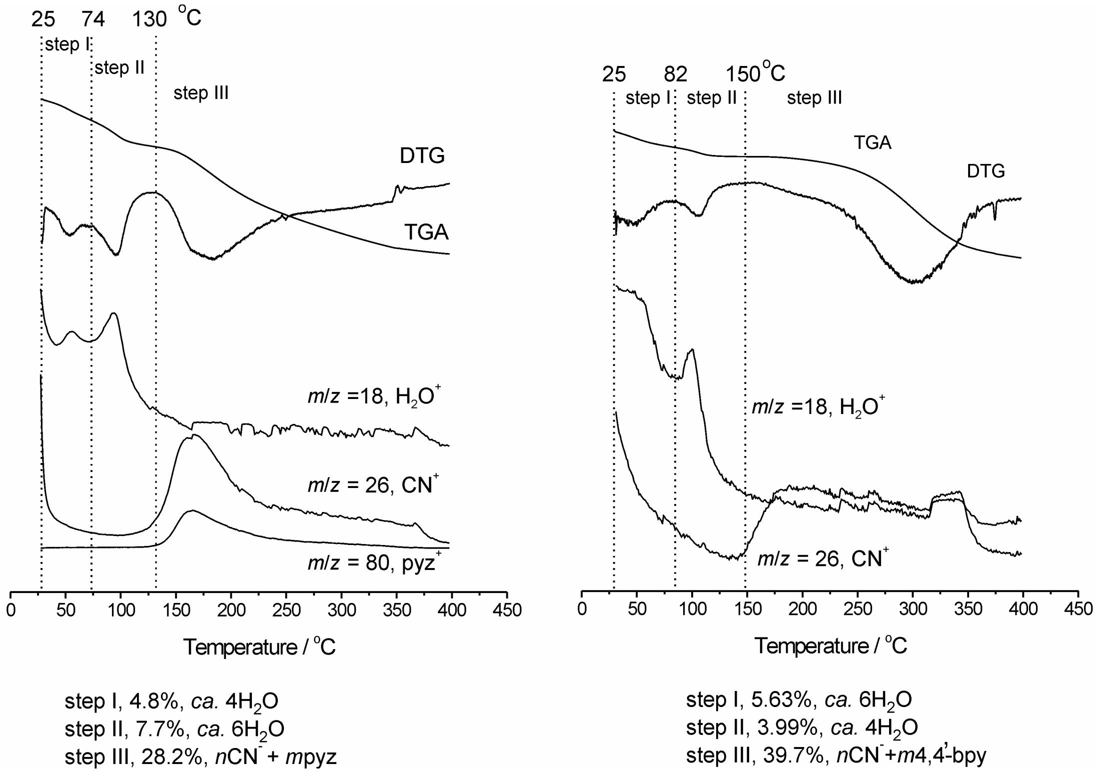

Figure S5. TGA coupled with QMS analyses for **1** (left) and **2** (right).

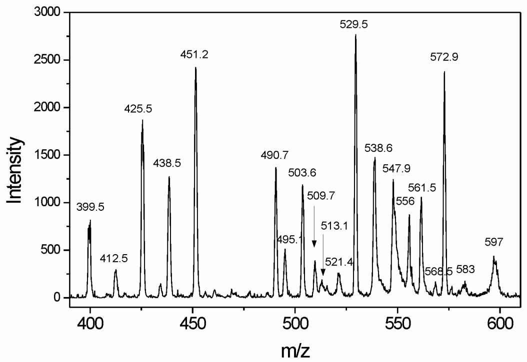

Figure S6. The fragmentation spectra of m/z = 607.88 band.

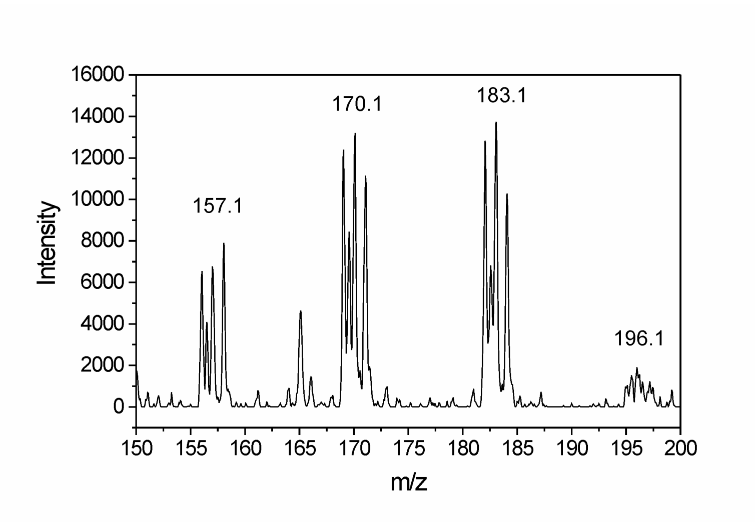

Figure S7. The representative fragment of ES-MS spectrum showing multi-lines bands assigned to set of doubly charged $[W(CN)_x]^{2-}$ species.

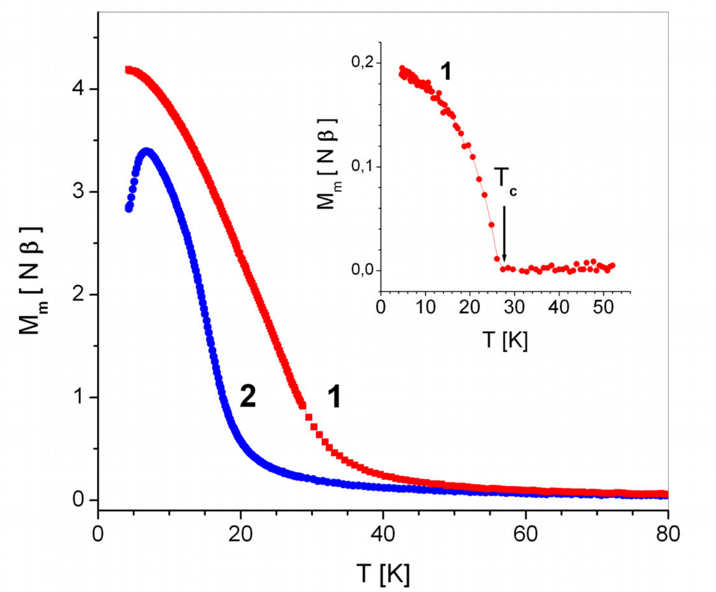

Figure S8. Thermal dependence of molar magnetisation for **1** and **2** measured at H_{dc} = 2 kOe. Inset: magnetisation change of **1** during the cooling of the sample in the field of superconducting magnet (ca. 10 Oe).